International Journal of Engineering and Technical Research (IJETR)
ISSN: 2321-0869 (O) 2454-4698 (P), Volume-13, Issue-1, January-June 2023

Effects of Equatorial Ionospheric Scintillation on GPS Coherent Carrier Phase Recovery

Daniel Anderson de Souza Leite and Antonio Macilio Pereira de Lucena

***Abstract*— GPS stands for Global Position System, this article aims to go into detail about this system, illustrating its specifications as a whole and specifically about a proposed Simulink GPS receiver model and its subsystems. The methodology used consists of exposing the theory on the subject and the architecture of the systems used. Multipath fading channel, ionospheric scintillation and coherent carrier recovery are discussed in depth. The Multipath Channel illustrates the path of electromagnetic propagation from orbiting satellites to the receiver in the vicinity of the Earth. Scintillation is the effect that the propagation suffers when passing through the ionosphere, the region which is located between the satellite and the receiver. Coherent carrier recovery deals with the function of the receiver in recovering the signal emitted by the transmitter. After building the GPS receiver model in question, validating and simulating the behavior of the receiver in an ionospheric scintillation environment, it was possible to carefully observe the performance of the receiver, how it behaves and how its parameters can change its reception quality.**

***Index Terms*— Ionosphere, Scintillation, Fading Channel, GPS coherent carrier recovery.**

I. INTRODUCTION

The Global Navigation Satellite System (GNSS) exist since the end of the 20th century. An example of this system is the NAVISTAR GPS, which was designed with the efforts of the US DoD. This system has a constellation of medium orbit satellites whose RF signals are sent from Outer Space to receivers near the globe. These RF signals propagate in such a way that a single GPS receptor can receive signals from multiple satellites by Code Division Multiple Access (CDMA) technology.

RF signals from Medium Earth Orbit (MEO) cross the entire Earth's atmosphere. The ionosphere; a layer of the atmosphere which contains free electrons and ions; diffracts, refracts and distorts the radio waves which pass through it. The signals which pass through the ionosphere undergo an effect called Ionospheric Scintillation. This effect causes fluctuations in amplitude and phase of these signals, as a result in the detection stage the receiving system can be led to a degraded performance or even the interruption of the link.

This paper aims to evaluate the performance of a GPS receiver system model, which was implemented in Simulink, under the effect of equatorial ionospheric scintillation. MathWorks Simulink is a platform for modeling, analyzing, and simulating systems.

A. Overview of GPS Signals

Each satellite in GPS constellation make use of two UHF links referenced by L1 and L2. Their frequencies are multiples of a fundamental frequency $f_0 = 10.23MHz$ based on [1].

$$f_{L1} = 154 \cdot f_0 = 1{,}575.42MHz \quad (1)$$
$$f_{L2} = 120 \cdot f_0 = 1{,}227.60MHz \quad (2)$$

The navigation data is modulated in baseband BPSK with 50bps. Soon after generated it is encoded by spread spectrum codes C/A and P(Y), then translated in frequency domain by the carriers L1 and L2. A schematic diagram is illustrated below.

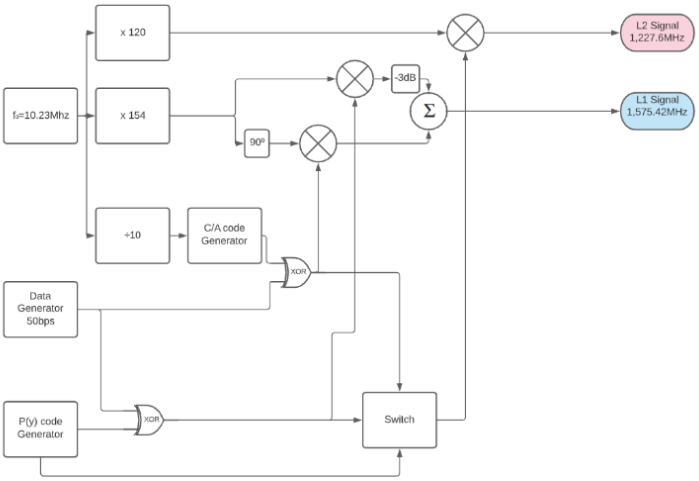

Figure 1 Signals generation schematic.

Figure 2 illustrates the process to generate the quadrature part of the modulated L1 carrier signal. The data signal and C/A code pass through Exclusive Or operation to give the C/A encoded signal which in turn modulates the sinusoidal part of the carrier.

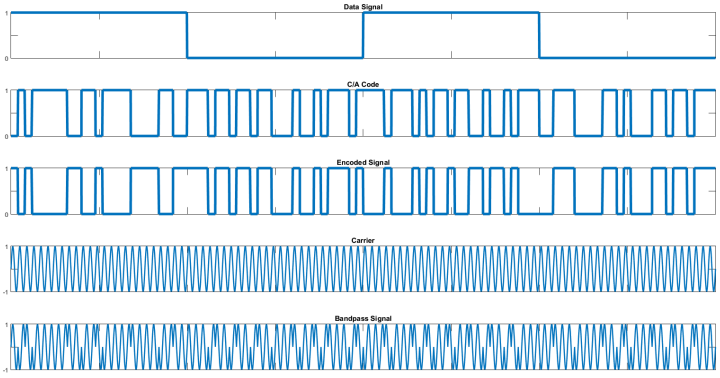

Figure 2 Time domain signals.

The C/A (Coarse Acquisition) code is performed by two 10-bit Linear Feedback Shift Registers, denoted by G1 and G2 generators, combined with a few logic operations as illustrated in figure-3. These registers implement 1023 chip-long sequences whose feedback configuration are defined by the following polynomials based on [1].

$$f(x)_{G1} = 1 + x^3 + x^{10} \quad (3)$$
$$f(x)_{G2} = 1 + x^2 + x^3 + x^6 + x^8 + x^9 + x^{10} \quad (4)$$

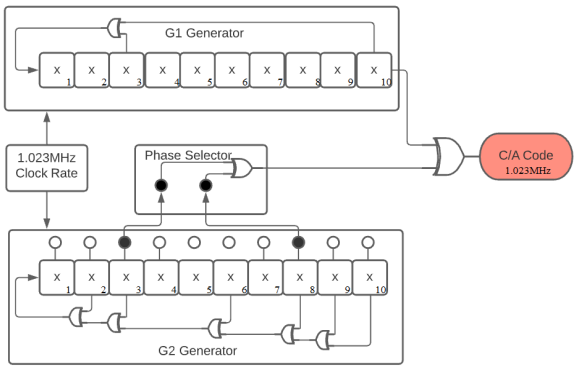

Figure 3 Spread Spectrum encoder.

The phase selector combines two outputs of G_2 generator to permit the generation of quite different C/A codes. The table-1 details the C/A codes for the 10 first satellites of the GPS system from [2].

Table 1. C/A parameters for 10 first GPS satellites.

Satellite ID number	GPS PRN Signal number	Code Phase Selection G2	Code delay Chips	First 10 chips Octal
1	1	2 ⊕ 6	5	1440
2	2	3 ⊕ 7	6	1620
3	3	4 ⊕ 8	7	1710
4	4	5 ⊕ 9	8	1744
5	5	1 ⊕ 9	17	1133
6	6	2⊕10	18	1455
7	7	1 ⊕ 8	139	1131
8	8	2 ⊕ 9	140	1454
9	9	3⊕10	141	1626
10	10	2 ⊕ 3	251	1504

B. *Ionosphere*

The earth's ionosphere is a layer of the atmosphere that is located approximately an altitude between 60km and 2,000km. It is composed of ions and free electrons, which can affect the properties of the electromagnetic waves that pass through it. The ionosphere is classified into sub-layers: D, E, F1 and F2. Each layer has its specificities in Chapter 8 in [3].

The ionospheric plasma is directly linked to the intensity of solar activity. Solar winds, coronal mass ejections, and other effects are capable to charge the ionospheric region.

C. *Ionosphere Scintillation*

Ionospheric scintillation is the effect, which the Ionosphere does on electromagnetic waves. The word has Latin etymology and comes from "scintillare" in the sense of to light up, to shine with intensity. A good analogy is the vibrating glow of the stars, which is compared with the variation of the envelope of electromagnetic waves passing through the ionosphere.

II. METHODOLOGY

This paper presents a theoretical background based on the referenced literature and proposes a model based in Simulink to make a GPS system operating over a channel under ionospheric scintillation. The receiver is evaluated through a figure of merit and its results are illustrated and compared in different scintillation contexts.

The figure of merit used illustrates the behavior of the receiver over a range of Carrier to Noise Density Ratio. The simulations performed observes the receiver behavior from the perspective of the receiver itself and the influence of scintillation on the receiver.

To make the results of the equatorial ionospheric scintillation on the carrier phase recovery clearer, two careful analyses are performed and presented in results.

All the parts used to implement the simulation from transmitter to the receiver are methodically described in the methodology subchapters below.

A. *Nav data and CDMA*

The navigation data is implemented by a Bernoulli binary generator with 0.5 probability between zero and one. Its generation frequency is 50 Hz equivalent to the 50 bps of navigation data GPS system. After generation, the data is modulated in baseband by a BPSK modulator that maps logical zero to +1 and logical 1 to -1 in [1].

C/A code generator, which performs the encoding and spectral spreading of the data for civilian use, C/A, is implemented in Simulink by two pseudo-random sequence generators, a delay block and the logic operations that were illustrated in figure 4 bellow.

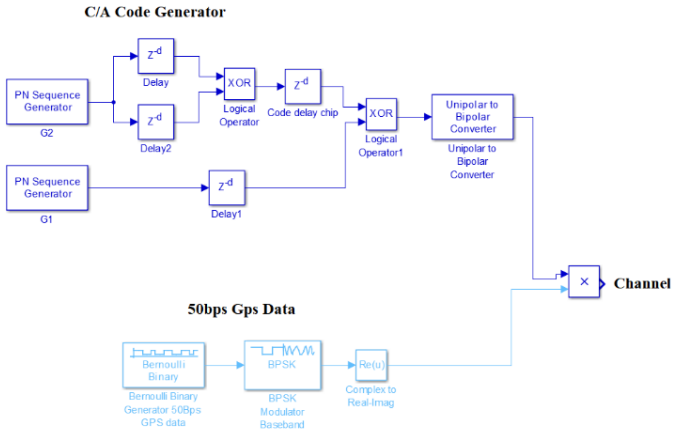

Figure 4 Nav data and C/A Code Generator.

In the figure 5 below we have the CDMA code set to a well-behaved frequency just for a better visualization of the code in the time domain. This C/A code actually does a chip rate of 1.023MHz in GPS system.

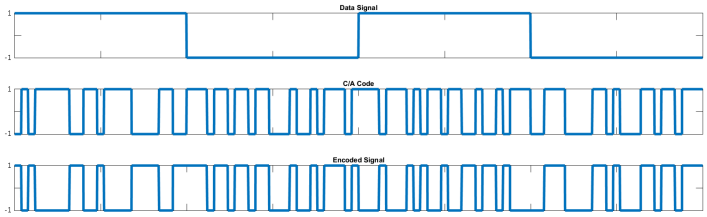

Figure 5 Nav data.

B. *Fading Channel Modeling*

A generic communication system can be modeled by the block diagram below.

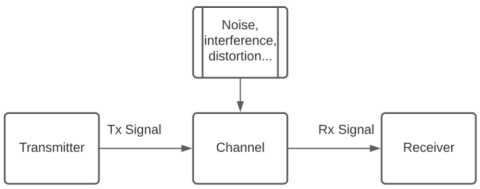

Figure 6 A generic communication system.

A wireless communication channel model is the medium between satellite and receiver, it can be, in our application, characterized by a Fading Channel. The energy of the propagating waves in this channel model which reach the receiver can be decomposed into two components. One is direct, specular, and the other is multipath, diffuse.

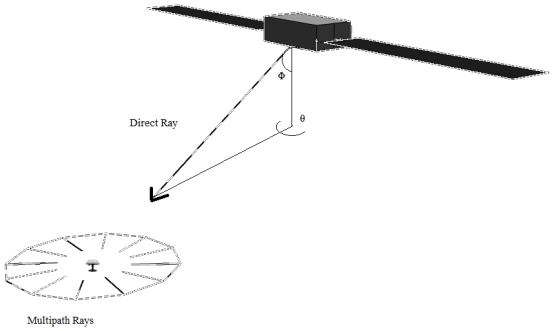

Figure 7 A wireless satellite communication channel.

According to Silva [4] and Simon et al. [5] when one component has more significant power than the others, the signal at the receiver has an envelope with a Rice distribution. The transmission coefficient, which modulates the transmitted signal is:

$$\tilde{z}(t) = \tilde{\bar{z}}(t) + \tilde{\xi}(t) \tag{5}$$

Whom,

$$\tilde{\bar{z}}(t) = A_0 e^{j(\omega_0 t+\theta_0)} = \tilde{\bar{z}}(t)_{\Re} + \tilde{\bar{z}}(t)_{\mathrm{im}} \tag{6}$$

$$\tilde{\xi}(t) = \sum_n^N A_n e^{j(\omega_n t+\theta_n)} \tag{7}$$

The $\tilde{z}(t)$ is a complex Gaussian process. Where $\tilde{\bar{z}}(t)$ is the direct component and behaves as a time-varying mean and $\tilde{\xi}(t)$ is the multipath component. The $\tilde{\xi}(t)$ has $n \in \mathbb{N}$ being the number of diffuse components and $\omega_n t + \theta_n$ are dependent the random variables azimuth, Doppler effect, and elevation of the angle of incidence. The average power of $\tilde{z}(t)$ is equivalent to the mean square value. Consequently, we have:

$$\Omega = \mathrm{E}\{\tilde{z}(t)^2\} = \mathrm{E}\{\tilde{z}(t)\tilde{z}(t)^*\} \tag{8}$$

$$\Omega = \mathrm{E}\{(\tilde{\bar{z}}(t) + \tilde{\xi}(t))(\tilde{z}(t)^* + \tilde{\xi}(t)^*)\} \tag{9}$$

$$\Omega = |\tilde{z}(t)|^2 + \mathrm{E}\left\{\left|\tilde{\xi}(t)\right|^2\right\} \tag{10}$$

However,

$$\mathrm{E}\{\tilde{\xi}(t)\} = \mathrm{E}\{\tilde{\xi}(t)_{\Re}\} = \mathrm{E}\{\tilde{\xi}(t)_{\mathrm{im}}\} = 0 \tag{11}$$

$$\mathrm{E}\left\{\tilde{\xi}(t)_{\mathrm{im}}{}^2\right\} = \mathrm{E}\left\{\tilde{\xi}(t)_{\Re}{}^2\right\} = \sigma^2 \tag{12}$$

$$\mathrm{E}\left\{\left|\tilde{\xi}(t)\right|^2\right\} = 2\sigma^2 \tag{13}$$

Hence,

$$\Omega = \left|A_0 e^{j(\omega_0 t+\theta_0)}\right|^2 + 2\sigma^2 \tag{14}$$

$$\Omega = {A_0}^2 + 2\sigma^2 \tag{15}$$

Being ${A_0}^2$ the average power of the direct component and $2\sigma^2$ the average power of the multipath component. The ratio of these powers is the Rice K parameter is given by:

$$K = {A_0}^2 \Big/ 2\sigma^2 \tag{16}$$

Considering that the real part of $\tilde{\xi}(t)_{\Re}$ is independent of $\tilde{\xi}(t)_{\mathrm{im}}$ the imaginary part and that $\tilde{\bar{z}}(t)$ is an average, we observe the joint probability density function of $\tilde{z}(t)$, where x is the real part and y the imaginary part.

$$pdf_{\tilde{z}(t)}(x,y) = \frac{1}{2\pi\sigma^2}\exp\left(-\frac{(x-\tilde{\bar{z}}(t)_{\Re})^2 + (y-\tilde{\bar{z}}(t)_{\mathrm{im}})^2}{2\sigma^2}\right) \tag{17}$$

$$pdf_{\tilde{z}(t)}(x,y) = \frac{1}{2\pi\sigma^2}\exp\left(-\frac{x^2+y^2+{A_0}^2-2(x\tilde{\bar{z}}(t)_{\Re}+y\tilde{\bar{z}}(t)_{\mathrm{im}})}{2\sigma^2}\right) \tag{18}$$

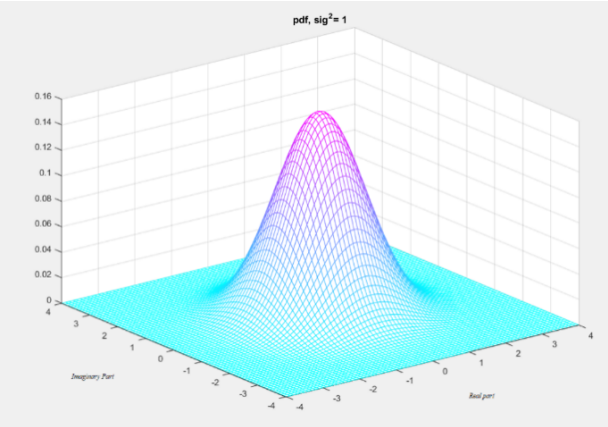

Figure 8 Probability density function of transmission coefficient.

Transforming the $pdf_{\tilde{z}(t)}(x,y)$ to polar coordinates $pdf_{\tilde{z}(t)}(r,\theta)$, with $x = \mathrm{r}\cos\theta$ and $y = r\sin\theta$, one observes:

$$pdf_{\tilde{z}(t)}(x,y) = \frac{1}{2\pi\sigma^2}\exp\left(-\frac{r^2 + {A_0}^2 - 2rA_0\cos(\omega_0 t + \vartheta_0 + \Theta)}{2\sigma^2}\right) \tag{19}$$

with $r \geq 0; 0 \leq \Theta \leq 2\pi$.

Thus, the probability density function of $|\tilde{z}(t)|$ is given by:

$$pdf_{|\tilde{z}(t)|}(r) = \int_0^{2\pi} pdf_{\tilde{z}(t)}(r,\theta)\, d\theta \tag{20}$$

$$pdf_{|\tilde{z}(t)|}(r) = \frac{r}{2\pi\sigma^2}\exp\left(-\frac{r^2+{A_0}^2}{2\sigma^2}\right) \cdot \int_0^{2\pi}\exp\left(-\frac{2rA_0\cos(\omega_0 t+\vartheta_0-\Theta)}{2\sigma^2}\right) d\theta \tag{21}$$

Note the integral function is periodic over θ, with period equal to 2π, the term $\omega_0 t + \vartheta_0$ is constant with respect to θ, thus we can make the following substitution:

$$I_0(x) = \int_0^{2\pi}\exp\left(x\cos(\phi)\right) \tag{22}$$

with $I_0(x)$ being the modified Bessel function of zero order. Therefore, we have:

$$pdf_{|\tilde{z}(t)|}(r) = \frac{r}{\sigma^2}\exp\left(-\frac{r^2+{A_0}^2}{2\sigma^2}\right)\cdot I_0\left(\frac{rA_0}{\sigma^2}\right) \tag{23}$$

where $r \geq 0$.

Rewrite it as a function of K, Ω and $r = \alpha$:

$$pdf_{|\tilde{z}(t)|}(\alpha) = \frac{2\alpha(k+1)}{\Omega}\exp\left(-k - \frac{\alpha^2(K+1)}{\Omega}\right) \cdot I_0\left(2\alpha\sqrt{\frac{k(k+1)}{\Omega}}\right) \quad (24)$$

where $\alpha \geq 0$.

Consistent with the equations above, this is the Nakagami-n distribution also known as the Rice distribution.

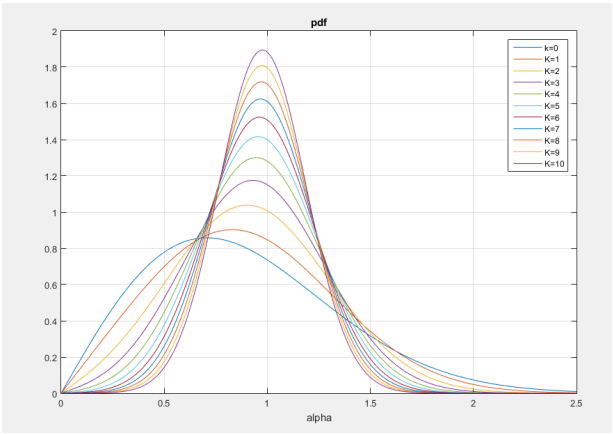

Figure 9 Probability density function of absolute value of transmission coefficient.

The channel illustrated above has a time-varying mean. This consideration makes this process non-stationary and more general. Our ionospheric scintillation generator in accordance with the Cornell model [6] makes use of a complex constant direct component.

C. *Mechanization of Scintillation*

The adopted model for scintillation generation is represented in figure 10, was based on [6]. This model has its essence in a complex white Gaussian process with zero mean and unit variance. Its components, real and imaginary, are generated independently and results in a complex process $\tilde{n}(t)$. This process is filtered by a 2nd-order Butterworth filter whose the magnitude response is given by:

$$|H(f)| = \sqrt{\frac{1}{1+\left(\frac{f}{B_d}\right)^4}} \quad (25)$$

$B_d = \frac{\beta}{(\tau_0\pi\sqrt{2})}$ is the filter bandwidth and $\beta = 1.2396464$. The decorrelation time τ_0 indicates the time value where the process autocorrelation is negligible. Therefore, the resulting process, denoted by $\tilde{\xi}(t)$, represents a complex filtered Gaussian noise.

On the other branch of figure 10, we have the complex constant $\tilde{\bar{z}}$ which is a direct component. The scintillation intensity is materialized through this component, and this is computed through the Rice K parameter and the scintillation index S_4. So, we have:

$$K = \frac{\sqrt{1-{S_4}^2}}{1-\sqrt{1-{S_4}^2}} \quad (26)$$

and for $S_4 \leq 1$,

$$\tilde{\bar{z}} = \sqrt{2K\sigma^2_{\tilde{\xi}(t)}} \quad (27)$$

Finally, these components are added to generate $\tilde{z}(t)$ and then it is normalized by the absolute value resulting in $z(t)$. Normalization is done to make the root mean square value, or average fading power, unitary on behalf of respecting the energy conservation theorem. $\Omega \equiv E\{|z(t)|^2\} = 1$.

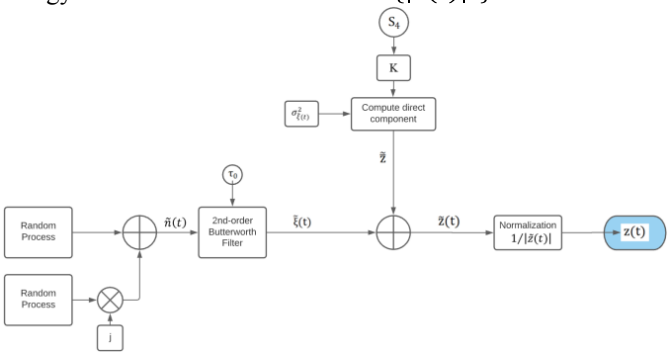

Figure 10 Mechanization of Scintillation.

1) *Scintillation Generator*

In our implementation, based on Cornell model [6] we choose an equatorial ionospheric scintillation situation with $\tau_0 = 0.27$ s and S_4 index varies by 0.2, 0.5 and 0.8. The methodology for simulating the scintillating channel was to generate the process $\tilde{\xi}(t)$ and obtain its current variance $\sigma^2_{\tilde{\xi}(t)}$ after the stability of the system. With the variance $\sigma^2_{\tilde{\xi}(t)}$ and the S_4 parameters the $\tilde{z}(t)$ was generated and then normalized by $|\tilde{z}(t)|$ to generate the transmission coefficient channel $z(t)$. The Simulink model to generate the scintillation signal is shown in the figure 11.

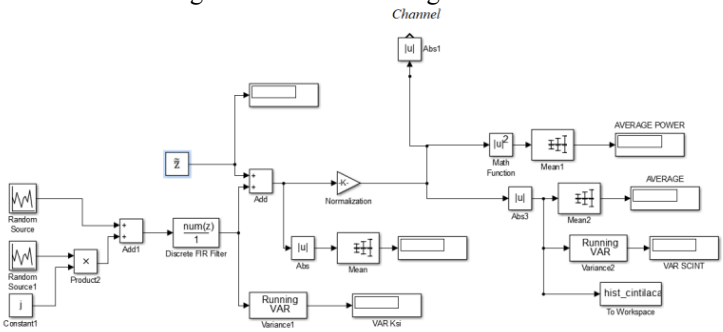

Figure 11 Scintillation Generator in Simulink.

Below it is presented some results of simulated signal $z(t)$. The magnitude (dB) and the phase (rad) of $z(t)$ is shown in the figure 12. The corresponding spectrum and magnitude histogram are illustrated in figure 13 and figure 14, respectively. The simulation was performed with index $S_4 = 0.8$, $\tau_0 = 0.27$ during a period of 60 seconds.

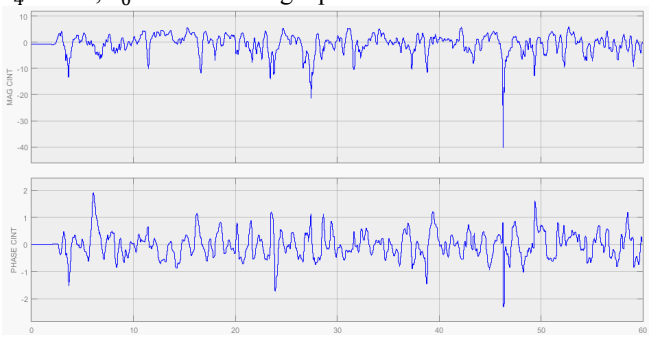

Figure 12 Scintillation in time.

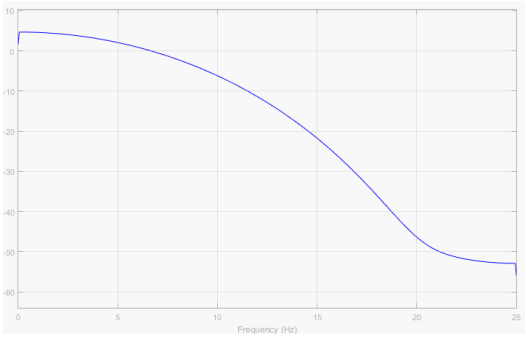

Figure 13 Scintillation spectrum.

In the illustration of histogram, there is a comparison with the Rise distribution, that is theoretical probability distribution for the magnitude of $z(t)$.

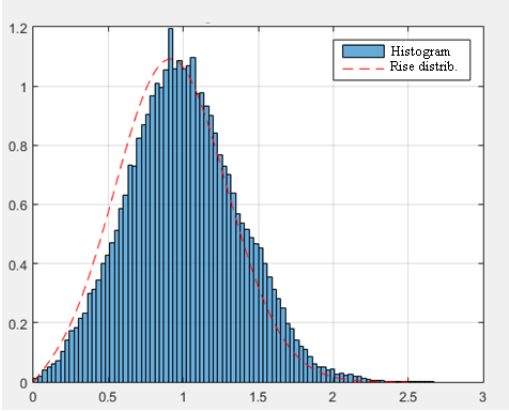

Figure 14 Histogram of scintillation magnitude.

D. GPS system description

The architecture of a GPS receiver on the L1 carrier, adapted from [1] follows in the diagram below.

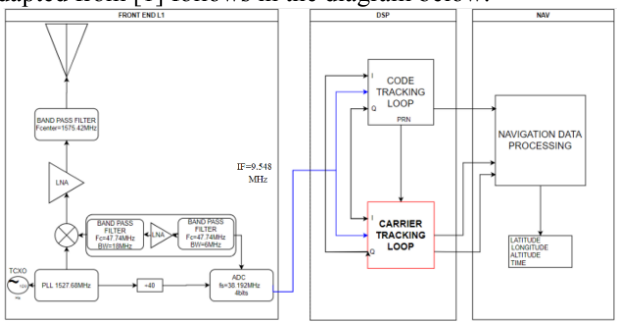

Figure 15 Architecture of GPS Receiver.

The front end is responsible for receiving electromagnetic waves at the L1 carrier frequency and converting them to IF (Intermediate Frequency).

The DSP (Digital Signal Processing) stage is responsible for sampling the IF signal and performing the processing capable of decoding, demodulating, and extracting the data needed by the NAV stage. The Code Tracking Loop and Carrier Tracking Loop sub-blocks are responsible for code tracking and carrier tracking, respectively.

The last sub-block NDP, Navigation Data Processing, performs the calculations to determine the geolocation of the receiver. Thus, summarizing the architecture required for a GPS receiver.

1) Carrier Tracking Loop (CTL)

The CTL used here is composed of a feedback classic circuit Costas Loop. It is responsible for demodulating the phase and quadrature signal components. Its structure implements a PLL (Phase Locked Loop).

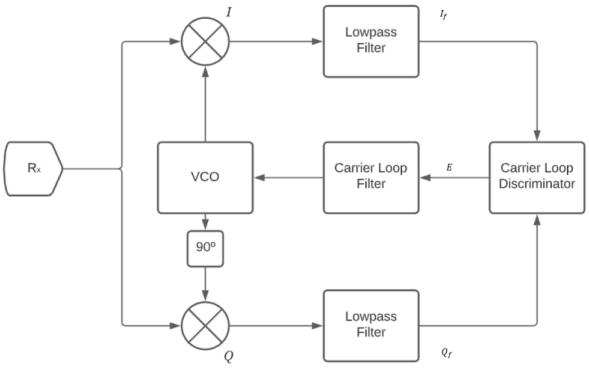

Figure 16 Costas Loop.

As noted in [1], three versions of this system are illustrated. For this purpose of this article, we focus on the PLL with discriminator proportional to $\sin(2\varphi)$. A brief analytical description of this circuit is performed in continuous time and the simile applies to discrete time. Following the indicated signals in Fig.16, we have:

Received Signal:

$$R_x = s(t) \cdot \cos(\omega_0 t + \varphi); \tag{28}$$

Upper branch (In-phase):

$$I = s(t) \cdot \cos(\omega_0 t + \varphi) \cdot \cos(\omega_0 t + \varphi'), \tag{29}$$

$$I = s(t) \cdot \left(\frac{\cos(\omega_0 t + \varphi) + \cos(\omega_0 t + \varphi')}{2} \right), \tag{30}$$

$$I = s(t) \cdot \frac{\cos(\varphi - \varphi')}{2} \cdot s(t) \frac{\cos(2\omega_0 + \varphi)}{2}; \tag{31}$$

After the low-pass filter (In-phase):

$$I_f = s(t) \cdot \frac{\cos(\varphi - \varphi')}{2}; \tag{32}$$

Lower branch (Quadrature):

$$Q = s(t) \cdot -\sin(\omega_0 t + \varphi) \cdot -\sin(\omega_0 t + \varphi'), \tag{33}$$

$$Q = s(t) \cdot \left(\frac{\sin(\omega_0 t + \varphi) + \sin(\omega_0 t + \varphi')}{2} \right), \tag{34}$$

$$Q = s(t) \cdot \frac{\sin(\varphi - \varphi')}{2} \cdot s(t) \frac{\sin(2\omega_0 + \varphi)}{2}; \tag{35}$$

After the low-pass filter (Quadrature):

$$Q_f = s(t) \cdot \frac{\sin(\varphi - \varphi')}{2}; \tag{36}$$

Central branch:

$$E = I_f \cdot Q_f = s(t) \cdot \frac{\cos(\varphi - \varphi')}{2} \cdot s(t) \frac{\sin(\varphi - \varphi')}{2}; \tag{37}$$

$$E = s(t)^2 \cdot \frac{\sin\left(2(\varphi - \varphi')\right)}{8}; \tag{38}$$

Since the domain of s(t) is 1 and -1. Then:

$$E = \frac{\sin(2\Delta\varphi')}{8}; \tag{39}$$

Invoking the small angle approximation, where $\sin(\phi) \cong \phi$, for $\phi < 0.244\, rad$, we can truncate the expression with error <1%.

$$E = \frac{\sin(2\Delta\varphi')}{8} \cong \frac{\Delta\varphi'}{4} = k \cdot \Delta\varphi'; \tag{40}$$

When, $\varphi \to \varphi'$. Making the difference $\Delta\varphi'$ an infinitesimal and k set to be unitary, we have:

$$E = k \cdot \Delta\varphi' \equiv d\varphi'; \tag{41}$$

Internally to the VCO, we have an integrator circuit, analytically:

$$\int d\varphi' = \varphi'; \quad (42)$$

This is the phase that controls the oscillator circuit. It is worth emphasizing that the circuit is a dynamic system and obeys all the convergence rules underlying it.

2) Phased Locked Loop

The Costa loop is equivalent to an PLL. This circuit is timeless in electronics and makes up many modern circuits. It is sub-composed of a loop filter and a VCO (Voltage Controlled Oscillator) in continuous time or a DCO (Digital Controlled Oscillator) for discrete time. The figures 17 e 18 illustrate the block diagram of an analog PLL.

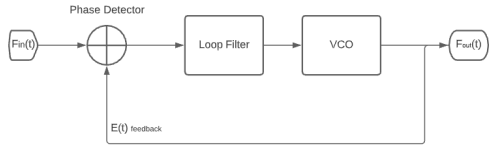

Figure 17 PLL in a continuous time domain.

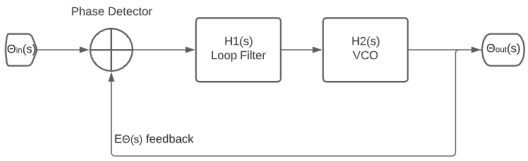

Figure 18 PLL in continuous frequency domain.

Based on [8], this circuit can be modeled using linear systems theory. Describing it in the continuous-time Laplace transform domain, we have:

Loop filter transfer function:

$$H1(s) = \frac{G_{loop}}{G_{loop} + s}; \quad (43)$$

Transfer function of the VCO integrator:

$$H2(s) = \frac{G_{DCO}}{s}; \quad (44)$$

Closed loop transfer function:

$$H_{cl}(s) = \frac{G_{loop}G_{DCO}}{s^2 + G_{loop}s + G_{loop}G_{DCO}}; \quad (45)$$

Function which is a second order system and can be rewritten as:

$$H_{cl}(s) = \frac{{\omega_n}^2}{s^2 + 2\zeta\omega_n s + {\omega_n}^2}; \quad (46)$$

Where the poles are determined by:

$$s_1 = -\zeta\omega_n + j\omega_n\sqrt{1-\zeta^2} \equiv \boldsymbol{\alpha + j\omega}, \quad (47)$$

$$s_2 = -\zeta - j\omega_n\sqrt{1-\zeta^2} \equiv \boldsymbol{\alpha - j\omega}; \quad (48)$$

Damping ration:

$$\zeta = \frac{\alpha}{\omega_n}; \quad (49)$$

Undamped Frequency:

$$\omega_n = \frac{8\zeta B_L}{4\zeta^2 + 1}; \quad (50)$$

Damping Factor:

$$\alpha = \zeta\omega_n; \quad (51)$$

Damped Frequency:

$$\omega = \omega_n\sqrt{1-\zeta^2}; \quad (52)$$

Settling Time:

$$t_s = \frac{4}{\zeta\omega_n}. \quad (53)$$

Since the goal is to obtain a digital circuit capable of being realized through software, the modeling must happen for discrete time z-transform values. According to [8], a DPLL implementation model:

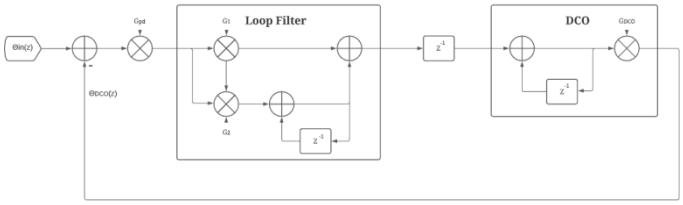

Figure 19 DPLL in z domain.

Loop filter transfer function:

$$H1(z) = \frac{G_1 + G_2 - G_1 z^{-1}}{1 - z^{-1}}; \quad (54)$$

DCO transfer function:

$$H2(z) = \frac{G_{DCO}}{1 - z^{-1}}; \quad (55)$$

Closed loop transfer function:

$$H_{CL} = \frac{G_{PD} \cdot H1(z)z^{-1} \cdot H2(z)}{1 + G_{PD} \cdot H1(z)z^{-1} \cdot H2(z)}, \quad (56)$$

$$H_{CL} = \frac{(g1 + g2)z - g1}{z^2 + (g1 + g2 - 2)z + (1 - g1)}; \quad (57)$$

Where $\boldsymbol{g1} = G_{PD} \cdot G_{DCO} \cdot G_1$ and $\boldsymbol{g2} = G_{PD} \cdot G_{DCO} \cdot G_2$.

$$g1 = 1 - e^{-2\zeta\omega_n T_s}, \quad (58)$$

$$g2 = 1 + e^{-2\zeta\omega_n T_s} - 2e^{-2\zeta\omega_n T_s}\cos(\omega_n T_s\sqrt{1-\zeta^2}); \quad (59)$$

Equivalent Noise Bandwidth:

Based on [9] for $H_{CL}(z) = \frac{b_1 z + b_2}{z^2 + a_1 z + a_2}$,

$$B_L = \frac{1}{2\pi j} \cdot \oint_{|z|=1} \frac{H(z)H(z^{-1})}{z} dz \equiv \frac{({b_1}^2 + {b_2}^2)(1 + a_2) - 2b_1 a_1}{(1 - a_2)[(1 + a_2)^2 - {a_1}^2]}; \quad (60)$$

Variance of the estimated recovered phase:

According to [9], [10], [11] the variance can be approximated by:

$${\sigma_\varphi}^2 \cong \frac{B_L T_{bit}}{c}; \quad (61)$$

Where $c = 10^{\frac{E_b/N_0}{10}}$, B_L in Hz and T_{bit} is the bit time in seconds.

E. Simulink receiver implementation

1) Carrier Tracking Loop

The demodulator is materialized by a Classic Costas Loop in Simulink. The closed loop transfer function is based on equation (57). The parameters used by the system are damping ratio $\zeta = 0.707$ and the equivalent noise bandwidth B_L set at 5, 10, 15 and 20Hz.

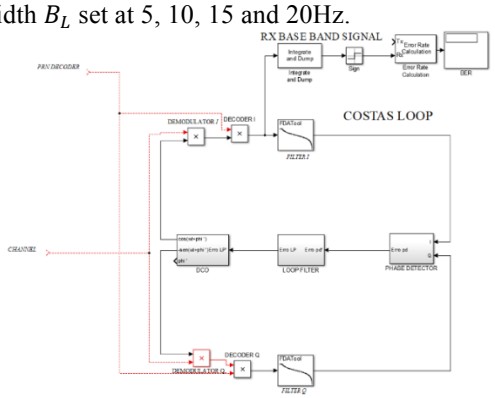

Figure 20 Costas Loop.

2) Phase error detector

After the phase detector mixer, a signal like eq. (40) $k_{pd} \cdot \Delta\varphi'$ is obtained. Considering the signal has added noise and the effects of the I and Q filters, the adjust of k_{pd} was performed by S-curve in an empirical way. The S-curve relates the expectation of the phase detector error $E\{k_{pd} \cdot \Delta\varphi'\}$ given a phase difference $\Delta\varphi'$ in such a way the angular coefficient of S-curve is unity. Thus, the output of the phase detector (Error pd) is the phase difference $\Delta\varphi'$.

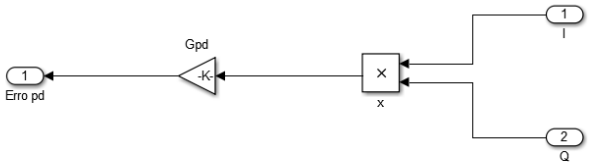

Figure 21 Phase error detector.

3) Loop Filter

The loop filter was implemented by eq. (54). The gains, g1 and g2, were obtained from equations (58) and (59). The output of Loop filter is a phase detector error filtered, Error lp.

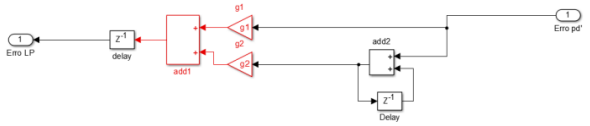

Figure 22 Loop Filter.

4) DCO

The DCO was implemented using eq. (55) with $G_{DCO} = 1$. The LUT, Lookup Table, inserts the estimated phase into the cosine and -sine functions as illustrated in the figure below.

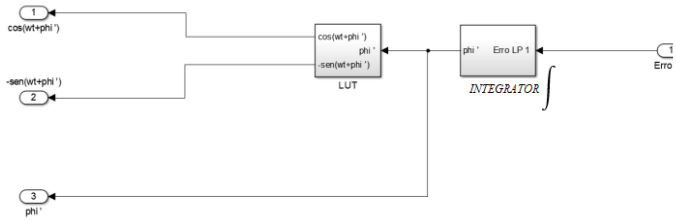

Figure 22 DCO.

F. *System validation*

To validate the receiver system implemented in Simulink, the methodology adopted was to compare the estimated recovered phase analytically by eq. 61 and simulated by the implemented receiver system. With the convergence of the comparison, the system is now validated and ready to evaluate the receiver response in context of ionospheric scintillation.

The proposed system is simulated by varying the Carrier to Noise Density Ratio from 25dB to 45dB and B_L set at 5Hz, 10Hz, 15Hz and 20Hz and determining the variance $(\sigma_\varphi{}^2)$ of the recovered phase.

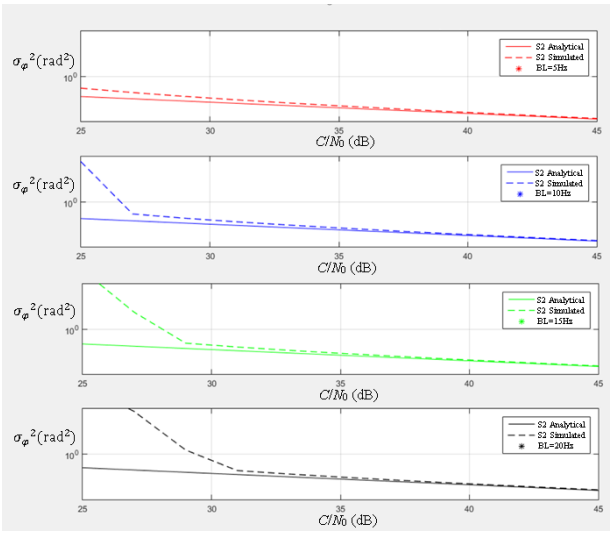

Figure 24 System validation.

III. SIMULATION RESULTS WITH SCINTILLATION

According to as proposed, the phase carrier recovery subsystem for GPS receiver is evaluate upon the influence of ionospheric scintillation. The figure of merit used to evaluate the receiver performance was the variance of the estimated phase recovered by the Costas loop. After the system is validated, the results can be seen in figure 25.

The idea is to evaluate the receiver behavior by varying the Carrier to Noise Density Ratio (C/N_0) from 25dB to 45dB with the S_4 index set at 0.2; 0.5; 0.8, and the Noise Bandwidth (B_L) at 5Hz, 10Hz, 15Hz, and 20Hz. All points on the graph were simulated for a period of 60 seconds, which was the time required for the figure of merit to converge.

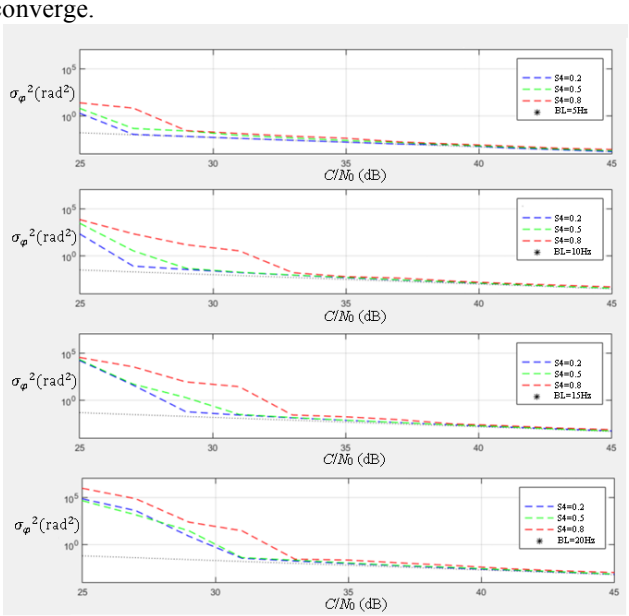

Figure 25 Results.

It is evident from the measurements that the figure-of-merit curves increases as the Carrier Power to Noise Density Ratio decreases. The noise equivalent bandwidth of the Costas Loop does the opposite effect decreasing the figure-of-merit the smaller its bandwidth is. A similar evaluation of GPS receiver performance can be found in [12].

A. Results Analysis

For a thorough analysis of the receiver, we present two analyses with the Carrier to Noise Density Ratio (C/N_0) taken to the extreme values. The first one considers the receiver in a low noise context, specifically with $C/N_0 = 45$ dB, illustrating the effect of scintillation and noise bandwidth on the receiver in the best case. The second takes the receiver in worst case, where the system fail in the high noise context.

For the first analysis we have the Table 2, here the figure-of-merit ($\sigma_\varphi{}^2$) is observed at an instantaneous, $C/N_0 = 45$ dB, of the results graph.

Table 2 $\sigma_\varphi{}^2$ at $C/N_0 = 45dB$

$C/N_0 = 45dB$	$S_4 = 0.2$	$S_4 = 0.5$	$S_4 = 0.8$
$B_L = 5Hz$	1.6E-4	2.0E-4	2.7E-4
$B_L = 10Hz$	3.6E-4	3.7E-4	5.0E-4
$B_L = 15Hz$	5.4E-4	5.5E-4	7.4E-4
$B_L = 20Hz$	7.1E-4	7.4E-4	1.1E-3

The second analysis is in the context of low C/N_0, evident for $C/N_0 < 35$ dB. To highlight the effect of scintillation on the receptor, three steps of $\frac{C}{N_0}$ scan was illustrated below performed in the context of S_4 index set at 0.2, 0.5, 0.8 with noise bandwidth (B_L) at 5Hz, 10Hz, 15Hz, and 20Hz in vicinity of the cycle slipping phenomenon in time domain. Cycle slip is a phenomenon that leads the system to fail and shows the difficulty over chasing the carrier in scintillation environment. In the graphs below we have on the left the variance of the phase estimated and on the right the phase estimated by Costas Loop over 60 seconds.

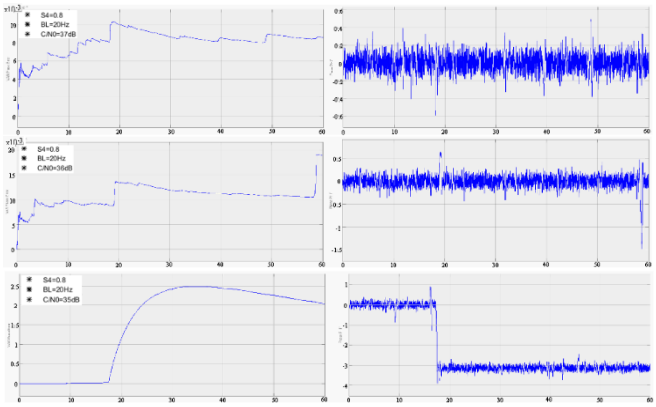

Figure 27 Three steps scan for $S_4 = 0.8$ and $B_L = 20Hz$.

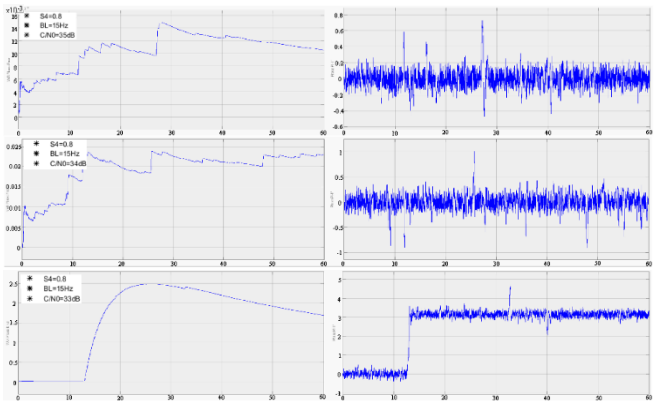

Figure 28 Three steps scan for $S_4 = 0.8$ and $B_L = 15Hz$.

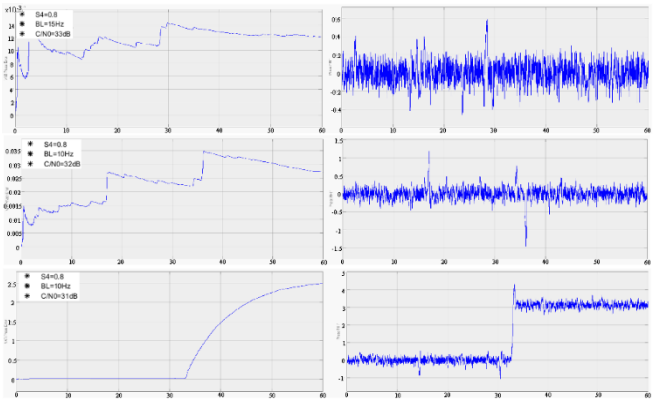

Figure 29 Three steps scan for $S_4 = 0.8$ and $B_L = 10Hz$.

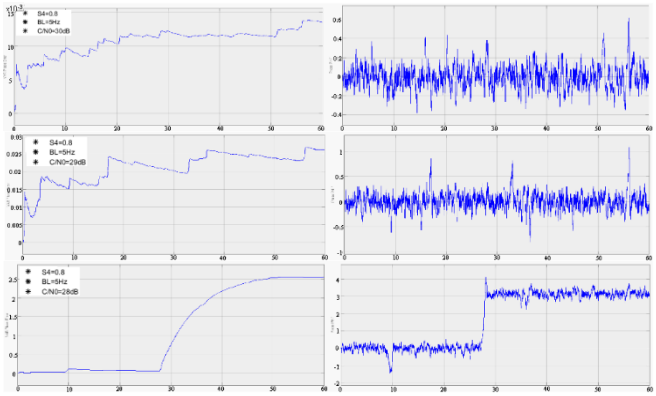

Figure 30 Three steps scan for $S_4 = 0.8$ and $B_L = 5Hz$.

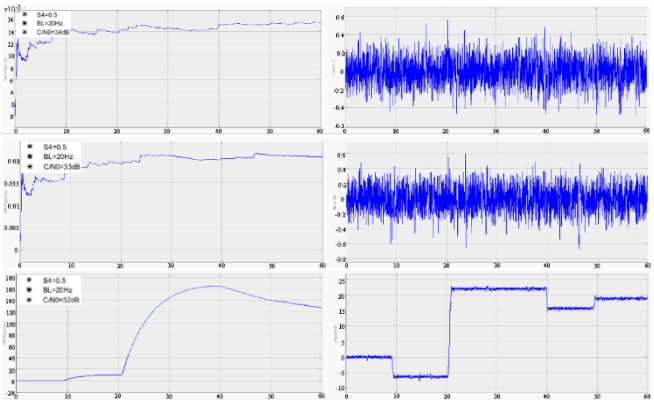

Figure 31 Three steps scan for $S_4 = 0.5$ and $B_L = 20Hz$.

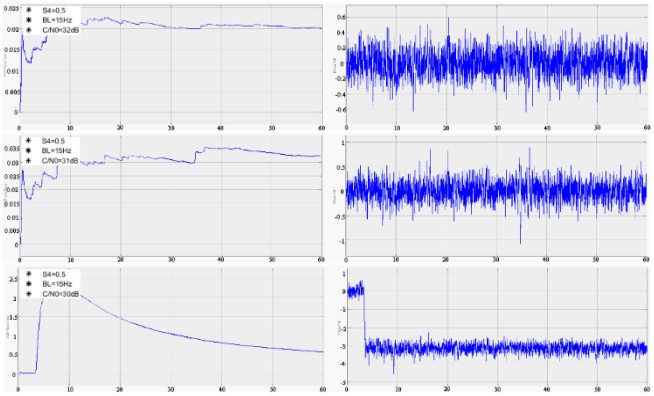

Figure 32 Three steps scan for $S_4 = 0.5$ and $B_L = 15Hz$.

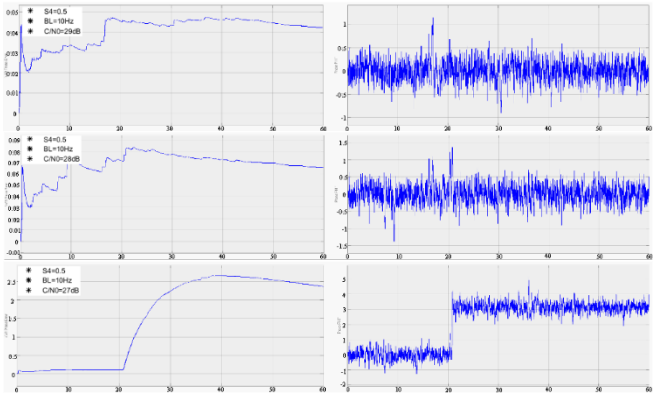

Figure 33 Three steps scan for $S_4 = 0.5$ and $B_L = 10Hz$.

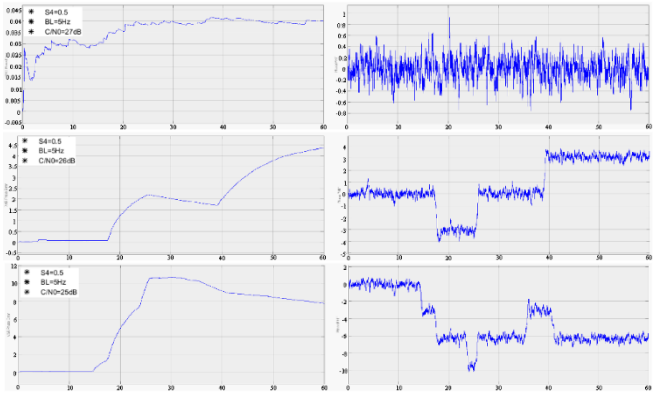

Figure 34 Three steps scan for $S_4 = 0.5$ and $B_L = 5Hz$.

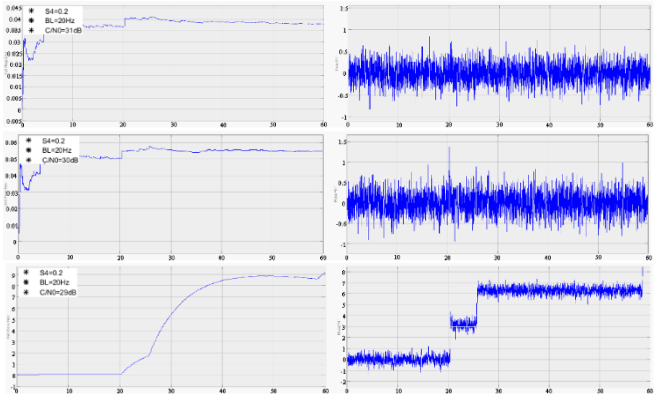

Figure 35 Three steps scan for $S_4 = 0.2$ and $B_L = 20Hz$.

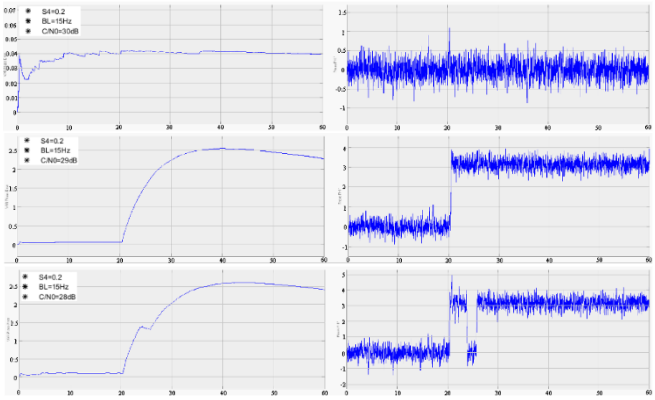

Figure 36 Three steps scan for $S_4 = 0.2$ and $B_L = 15Hz$.

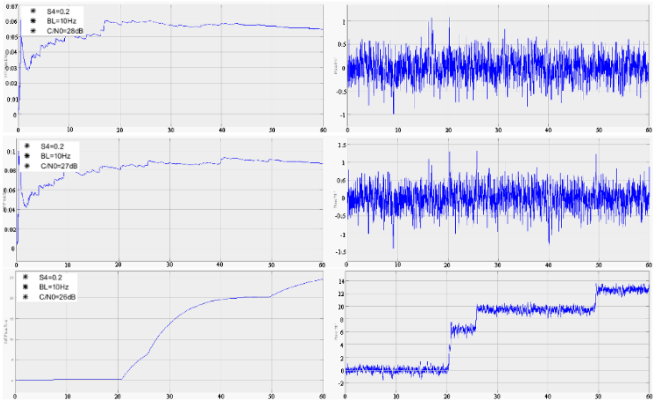

Figure 37 Three steps scan for $S_4 = 0.2$ and $B_L = 10Hz$.

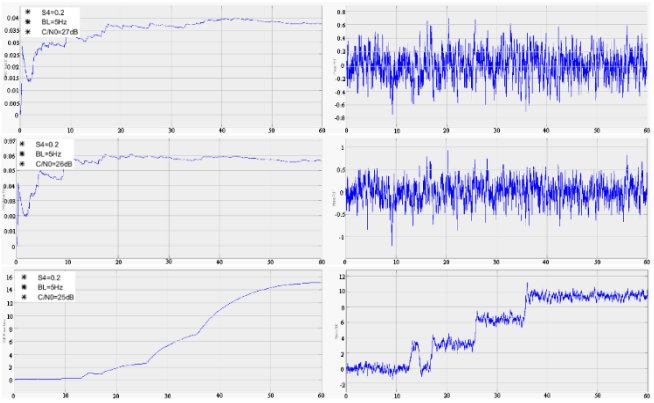

Figure 38 Three steps scan for $S_4 = 0.2$ and $B_L = 5Hz$.

IV. Conclusion and Remarks

This paper presented ionospheric scintillation and its interaction with GPS signals in a proposed receiver implemented in Simulink. The synthesis of the scintillation was based on Cornell's model [6]. The receiver used was based on [1] and its circuits were appreciated mathematically. The receiver analysis was focused on the carrier tracking subsystems and generated an evaluation on the receiver behavior in the context of ionospheric scintillation.

To characterize the reception quality, a figure of merit, the variance of the phase estimate by Costas loop, was adopted, which behaved as a good parameter to evaluate the performance of the reception stage. The first evaluation considered the Carrier to Noise Density Ratio (C/N_0) in a good context with variations of the scintillation intensity and noise bandwidth of the Costas loop, which resulted an order of magnitude of the figure of merit of 10^{-3}. In this way the scintillation was not able to be damage the carrier recovery.

The second analysis, in the low Carrier to Noise Density Ratio (C/N_0) context, was more thorough, where a scan of the C/N_0 was performed and chosen appropriately. As the results showed, for a fixed scintillation index, it can be observed that the carrier recovery was more robust according to the noise bandwidth of the circuit was smaller. Exempli gratia, for a fixed $S_4 = 0.8$, with $B_L = 20Hz$ the system failed at $C/N_0 = 35$ dB, while with $B_L = 5Hz$ the failure only occurred at a density of $C/N_0 = 28\ dB$. On the other hand, the behavior of the receiver at a fixed noise bandwidth, it can be observed that the higher scintillation index, the more damaging it is for the system to recover the carrier. Exempli gratia, with a fixed noise bandwidth

$B_L = 5Hz$, for a $S_4 = 0.2$ the receiver failed at $C/N_0 =$ 25 dB, while with $S_4 = 0.8$ the failure was only observed at $C/N_0 = 28$ dB as expected. Another characteristic of the GNSS carrier recovery subsystem is the occurrence of cycle slip when increases the value of S_4 or the C/N_0 drops.

Therefore, one can observe that scintillation was extremely harmful to the receiver in low Carrier to Noise Density Ratio (C/N_0) context and the noise bandwidth of Costas loop directly influences the scintillation robustness.

ACKNOWLEDGMENT

We thank the Federal Institute of Education, Science and Technology of Ceará (IFCE), the National Institute for Space Research (INPE) and Fortaleza University (Unifor) for all support given to this work.

REFERENCES

[1] K. Borre *et al., A software-defined GPS and Galileo receiver: Single-frequency approach*. Boston: Birkhäuser, 2007.
[2] A. Flores, "NAVSTAR GPS Space Segment/Navigation User Segment Interfaces," GPS Enterprise Space & Missile System Center, El Segundo, CA, Report No. IS-GPS-200, 2020.
[3] Y. Kamide and A. Chian, *Handbook of the Solar-Terrestrial Environment*. Berlin, Heidelberg, NY: Springer, 2007.
[4] V. A. da Silva, "Modelagem computacional de canais de comunicação móvel" [Computational modeling of mobile communication channels]. M. S. thesis, USP. São Paulo, SP, 2004.
[5] M. K. Simon and M. Alouini, Digital Communication over Fading Channels: A Unified Approach to Performance Analysis. New York, NY: John Wiley & Sons, INC, 2000.
[6] T. E. Humphreys, "Modeling Ionospheric Scintillation and Its Effects on Gps Carrier Tracking Loops and Two Other Applications of Modeling and Estimation," Ph. D. dissertation, Cornell University, Ithaca, NY, 2008.
[7] T. E. Humphreys, M. L. Psiaki, J. C. Hinks, B. O'Hanlon and P. M. Kintner, "Simulating Ionosphere-Induced Scintillation for Testing GPS Receiver Phase Tracking Loops," in *IEEE Journal of Selected Topics in Signal Processing*, vol. 3, no. 4, pp. 707-715, Aug. 2009, doi: 10.1109/JSTSP.2009.2024130.
[8] B. W. Li. "Introduction to phase-locked loop system modeling." *Analog Applications Journal*, pp. 5-11. May 2000.
[9] W. C. Lindsey and Chak Ming Chie, "A survey of digital phase-locked loops," in *Proceedings of the IEEE*, vol. 69, no. 4, pp. 410-431, April 1981, doi: 10.1109/PROC.1981.11986.
[10] A. S. Silva and A. M. P. Lucena, "Demodulador OQPSK: Implementação completamente digital para aplicações espaciais" [OQPSK Demodulator: Fully digital implementation for space applications]. Novas edições Acadêmicas. https://bityli.com/bBLtFX
[11] A. M. P. de Lucena and D. A Costa. "Quadrature decomposition of the discrete and stochastic processes" Submitted to *2019-2020 Anais da Academia Cearence de Matemática*, 2020.
[12] A. O. Moraes, W. J. Perrella. "Performance evaluation of GPS receiver under equatorial scintillation," in *Journal of Aerospace Technology and Management*, vol. 1, no. 2, 193–200, Dec. 2009.
[13] A. A. Giordano and A. H. Levesque, *Modeling of Digital Communication Systems Using Simulink*. Hoboken, NJ: Wiley, 2015.
[14] M. K. Simon, Probability Distributions Involving Gaussian Randon Variables: A Handbook for Engineers, Scientists and Mathematicians. New York, NY: Springer, 2006.
[15] *Ionospheric propagation data and prediction methods required for the design of satellite services and systems,* ITU-R Recommendation P.531-6, 2001
[16] P. M. Kintner, M. B. Ledvina and E. R. De Paula. "GPS and ionospheric scintillations." *Space Weather*, vol. *5, no.* 9, pp. 1-27, Sep., 2007. [Online]. Available: https://doi.org/10.1029/2006SW000260
[17] "Solar Cycle 25 Forecast Update." Space Weather Prediction Center. https://www.swpc.noaa.gov/news/solar-cycle-25-forecast-update (accessed Feb. 25)…
[18] J. G. Proakis. *Digital Communications*. McGraw-Hill. 4th ed. New York, NY 2001.
[19] V. di Santis, "Simulação e análise dos efeitos da cintilação ionosférica em um receptor de GPS utilizando a modulação DPSK"[Simulation and analysis of the effects of ionospheric scintillation on a GPS receiver using DPSK modulation]. M. S. thesis. ITA.São José dos Campos, 2013.

Daniel A. S. Leite received the BS degree in Telecommunications Engineering from Federal Institute of Education, Science and Technology (IFCE), Fortaleza, CE, Brazil. He did his course conclusion over ionospheric scintillation, modulation, signal processing and coherent carrier recovery.

Antonio Macilio Pereira de Lucena received the BS degree in Electronics Engineering from Technological Institute of Aeronautics (ITA), São José dos Campos, SP, Brazil, in 1980, the MS degree in Space Telecommunications and Electronics from National Institute for Space Research (INPE), São José dos Campos, SP, Brazil, in 1986, and the Doctor degree in Teleinformatics Engineering from Federal University of Ceará (UFC), Fortaleza, CE, Brazil, in 2006. He worked at INPE from 1983 up to 2022 where he has been involved in various projects in the areas of satellite communications, electronics, and radio-astronomy. Since 2007, he is also professor at University of Fortaleza (UNIFOR), Fortaleza, CE, Brazil. His present research interests include modulations, space communications, signal processing, and communication theory.